3

Adipose Measurement Using Micro MRI

Yang Tang and Rex A. Moats
University of Southern California, Children's Hospital Los Angeles
USA

1. Introduction

The increased incidence of obesity and well-documented co-morbidities, have lead to the recognition that obesity is a public health epidemic (Mann, 1974; Larsson et al., 1984). Excess adipose tissue is a high risk factor for cardiovascular and metabolic syndrome (Manson et al, 1990). These two diseases both rank high on the list of leading causes of morbidity and mortality not only in the developed world but now also in the developing world..

The now well established relationship between excess adiposity and disease, has spurred obesity research which has been supported both by public institutions and private companies. In most of adiposity research, the experiment designs require the assessment of the adipose load and the development of the associated biological or medical issues. The measurement of fat tissue is a fundamental task. Studies covering both the nature history of obesity and the development of obesity associated diseases often require repeated longitude measurements during the course of the experiments. This is especially true of protocols assessing interventions through outcome analysis. This chapter focuses on the measurement of adipose tissue in animal models by micro MRI in combination with an automated method for adipose measurement. The emphasis is on the logic, development and application of the computational methodology for virtual fat extraction.

1.1 Adipose imaging technique

Classic adipose measurements have been based on weight or Body Mass Index (BMI). Recently imaging technologies have emerged as powerful tools for refined adipose assessment (Zhao et al., 2006; Luu et al., 2009). Imaging can provide not only the size of an adipose depot, but also its location. Often this more accurate information is of critical importance to the adipose researches.

For adipose measurement, a variety of imaging techniques have been adopted in both human beings and small animals. Computed tomography (CT) is a widely used technique. It has the merits of high resolution and low cost. It has been developed in both humans (Zhao et al., 2006; Ohshima et al., 2008) and animals (Luu et al., 2009; Lublinsky et al., 2009). Compared to CT, Magnetic Resonance Imaging (MRI) (Gray, 1991; Gronemeyer, 2000) has advantageous in adipose research. Because MRI is radiation free, it is good for radiation sensitive research and desirable for longitudinal studies where the effects of radiation would be additive. This is especially true at the high resolution covered here.

1.2 Animal model and micro MRI

Experiments on Human subjects have obvious appropriate limitations. The mouse has emerged as the human surrogate in a large body of obesity research. In drug development and translational medicine research, preclinical research of animal models plays a significant role. Thus, researchers studying adipose tissue and the associated disease processes are actively pursuing preclinical studies using mouse models (Bechah et al., 2010; Church et al., 2009).

Micro MRI (small animal MRI) is a powerful tool for in vivo fat measurement using small animal models. As described before, micro MRI can provide quantitative information about fat volume as well as depot locations (Ranefall et al., 2009). In adipose research it is often important to obtain spatial information related to the mechanism of pathogenesis and disease onset.

1.3 Post processing

1.3.1 Manual measurement

Although micro MRI provides a powerful imaging tool, the post processing of the image dataset is intense time consuming work for both technicans and experts. Especially, for accurate abodomial adipose measurement, 3D volume instead of 2D slices are obtained for each animal. Therefore, a typical experiment on a group of mice will generate thousands of images requiring adipose measurements. This is an obstacle for high throughput and efficient discovery. In order to get the exact adipose region, manual drawing Region of Interests (ROI) is usually carried out. In such procedures, the errors and variations are inevitable.

In the case of manual measurements, intra- and inter-operators' variations result in repeated measurements and statistical complexity. Furthermore adipose tissue has irreguar shapes and located in various depots throughout the body. Thus expertise are required to detect the adipose from the organs in the MRI images. All these factors decrease the accuracy for fat measurement.

1.3.2 Automatic measurement

Considering the above limitation and complexity added by manual analysis, automated or semi-automated techniques are urgently demanded for adipose measurements which can relieve the researcher from the tedious operational burdens as well as reduce the operator-dependent errors.

In order to accomplish automatic measurement, many tasks have to be considered.

For fat measurement, the total size and locations of the fat tissues is basic information needed. From the imaging and image-processing viewpoint, how to extracting the fat pixels from the MR image is the first task.

This task require matched and optimized imaging protocols and customized algorithms. Based on the observation that fat is relative bright in T1 weighted images, the adipose tissues are often extracted from the images by applying a threshold to the intensities (Ranefall et al., 2009; Sijbers et al.,1998; Chae et al., 2007). To deal with the inhomogenity of the MR images due to the inhomogeneitis in the magnatic field, local and adaptive threshold methods have been adapted (Sijbers et al.,1998; Chae et al., 2007). Beyond threshold based

methods; fuzzy logic methods have been applied. In fuzzy logic, each pixel is assigned a fuzzy membership to indicate the probability that the pixel is fat. Then the fat is extracted by minimizing the membership function instead of being based solely on a threshold (Positano et al., 2004; Positano et al., 2009). More mathematically complex models have been created to compensate for the inhomogeneities in the intensity images (Hou, 2006; Vovk et al., 2007). But methods based only on intensity are in general limited because other tissues or objects in the background exhibit similar intensities and complicate the separation. An exmaple can be seen in Figure.1, where the fat and non-fat region are close in intensity. (Tang et al., 2011)

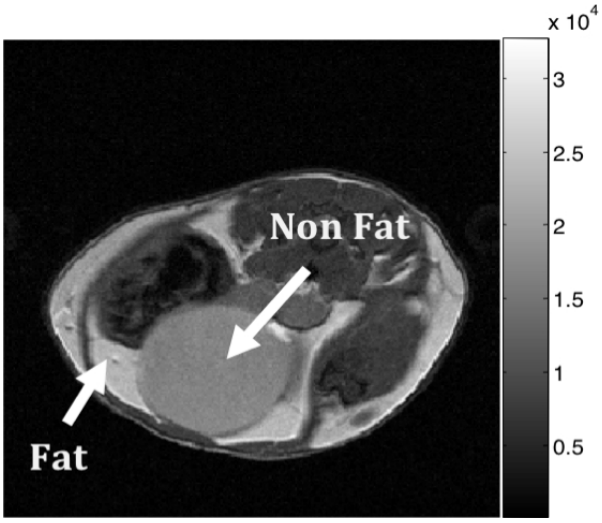

Fig. 1. The similar intensity of fat and non fat pixels in this case in the bladder. (Tang et al., 2011)

As a result, image acquisition techniques have been proposed to provide better discrimination. For example, the water-saturation technique (Dixon et al., 1984; Reeder et al., 2005; Peng et al., 2005). However, analogous techniques have not been implemented for small animals at micro MRI due to magnetic field inhomogeneities at high field that can lead to artifacts and due to the increased difficultly of implementing strictly analogous pulse programs.

For fat measurement, the location of fat depots has been shown to provide important information relevant to disease states. For example, the amount of abdominal visceral fat has been shown to be related to hypertension and cardiovascular disease, cerebrovascular disease, insulin resistance and type 2 diabetes (Ross et al., 2002; Snijder et al., 2006). Thus, an important issue in fat analysis is to assign the fat depot type to associated anatomical location, which usually includes the subcutaneous fat and visceral fat. To identify different fat depots, one common methods is based on region growing algorithms (Siegel et al., 2007; Ranefall et al., 2009), which start from the seed points planted in the different fat depots and grow to include nearby pixels with similar intensity into the same group and therefore depot. But the region growing method is difficult to apply in thin mouse with scattered fat tissues. Automated placement of the seed is still an unmet challenge in most cases.

In order to separate the visceral and subcutaneous fat, curve deformation methods (Positano et al., 2004; Positano et al., 2009; Zhao et al., 2006) have also been reported. These methods

deform a curve inwards from skin contour to locate a muscle layer. Because the muscle layer lies between the subcutaneous and visceral fat, the different fat depots are separated by default.

1.4 Automatic fat measurement on micro MRI

Fat measurements using imaging technique have been established in humans (Siegel et al., 2007; Ohshima et al., 2008) at lower field strengths, fat measurement in mice models using micro MRI has not been adequately addressed.

Here we summarize our fat measurement system using micro MRI. As the schematic representation illustrated in Figure 2, the system includes an imaging and post processing module. In the imaging module, the mice are subject to a MRI scanning on the abdominal region with multiple echo sequence. In the post processing module, fat is first extracted from the multiple echo images with a multi-part algorithm based both on intensities and each pixels T2 translation relaxation time. In our system, the fat extraction is accomplished by adopting a fuzzy c mean clustering algorithm in the T1 weighted image and then selecting clusters into fat regions aided by the additional T2 information.

For fat depot recognition, we developed a method which utilizes a knowledge-based framework for image post acquisition image processing, which takes advantages of the a priori anatomical knowledge and automatically segments each depot into visceral fat or subcutaneous fat using fuzzy logic techniques.

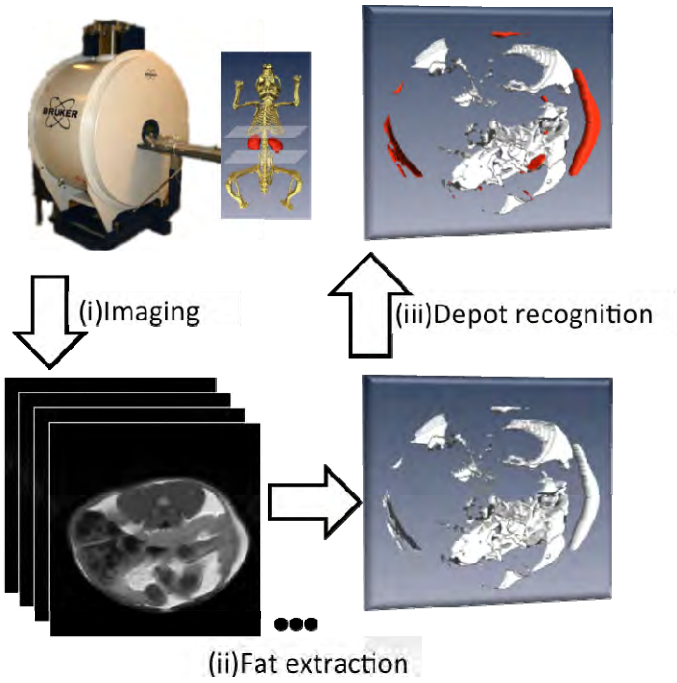

Fig. 2. The schematic representation of adipose measurement system using micro MRI

In this chapter, we will describe how we perform the fat measruement in typical mouse model of obseity, detailing how to perform the imaging, fat extraction and depot separation. Most of the content of this chapter comes from our groups previous and ongoing research work (Tang et al., 2010; Tang et al., 2011). For each section, section 2 presents the imaging protocol and animal groups for image acquisition; section 3 introduces the fat extraction method; section 4 describes the depot separation algorithm. In section 5, the automatic results is compared to manual reference for validataion. After that, the conclusion and acknowledgement is given in section 6 and section 7 respectively.

2. Image acquisition

2.1 Imaging sequence on micro MRI

The experiments were performed on micro MRI scanner (70/16 Bruker PharmaScan, Germany). The field strength of the instrument is 7.05 Tesla and the maximal gradient strength is 400mTesla/m.

To provide adequate signal to noise and coverage, slices were collected with 1mm thickness. An optimized Bruker multiple-slice-multiple-echo (MSME) sequence (TR=5300ms, TE=12~120ms, 10 echoes) was adopted to get the high signal to noise ratio. The field of view was 3*3cm and matrix size was 256*256, in-plane resolution was 117um.

In the imaging, we focus on the abdominal fat. For this purpose, mice were placed prone in a semi cylindrical holder. In previous research (Luu et al., 2009), the abdominal region has been defined from L1 to L5 of the spine in the CT images. Because in the MRI, bone hypointense is not as easily differentiated as it is in the CT, we define the abdominal region in micro MRI using the kidneys as a reference. Data starts at the slice at the top of the left kidney and ends at the end of right kidney.

2.2 Animal population

In order to validate the measurement system, the experiments were tested on an animal population with 26 wild type C57BL/6 mice.

There are 4 groups in the mice population with different adipose ratio, which is differentiated by feeding strategies. Mice received regular chow or a high fat diet respectively. In the regular chow group, mice were placed into 3 litters with different sibling numbers that provided different nutritional conditions due to competition or lack of competition. The details of animal experiments are listed in Tab.1 including large litter (LL), normal litter (NL), small litters (SL) and high fat (HF) groups. (Tang et al., 2011)

Group	Mouse num (Male, Female)	Feed	Little	Sibling num
LL	M=6 F=1	Chow	LL	12
NL	M=4 F=1	Chow	NL	7
SL	M=7 F=2	Chow	SL	3
HF	M=2 F=3	High Fat	LL,NL,SL	5

Table 1. Animal population for the experiments (Tang et al., 2011)

3. Adipose extraction

3.1 Principle

In the MR image, due to the high proton density, fat tissues usually has relative high intensity values. But only intensity information is not sufficient to allow segmentation due to complicated mechanisms resulting in high intensities in other organism as well. Therefore in the multi-component method, we combine pixel intensity information with transverse relaxation time to aid in the automated extraction of the fat tissues.

The basic idea is illustrated in Figure 3 (Tang et al., 2011). Here the first echo image is selected because of its high signal to noise ratio(SNR) compare to other echo images. In the first echo image, instead of the explicit threshold, the fuzzy c means (FCM) clustering approach (Dunn, 1973) is adopted to classify all pixels into groups. With the cluster image, we can first exclude the mouse body from the background by sorting the average intensity in each cluster. The cluster with their average intensity less than minimium threshold is considered to be background.

To deal with problem of the non fat tissue with high intensity in the T1 weighted image, the T2 parametric image based primarily on relaxation is explicitedly calculated from the multiple echo images. Because the T2 value reflects the transverse relaxation time of tissues, the T2 parametric image can help to separate the fat and non-fat tissues. An example is displayed in Figure 4, where the T2 parametric image exhibits a larger range of statitstially distinguishable values and thus aids us in seperating the fat from the non-fat tissues.

Prior to the fat extraction, an image filter is applied to the image data to reduce the noise level. All the technical details are summarized as following.

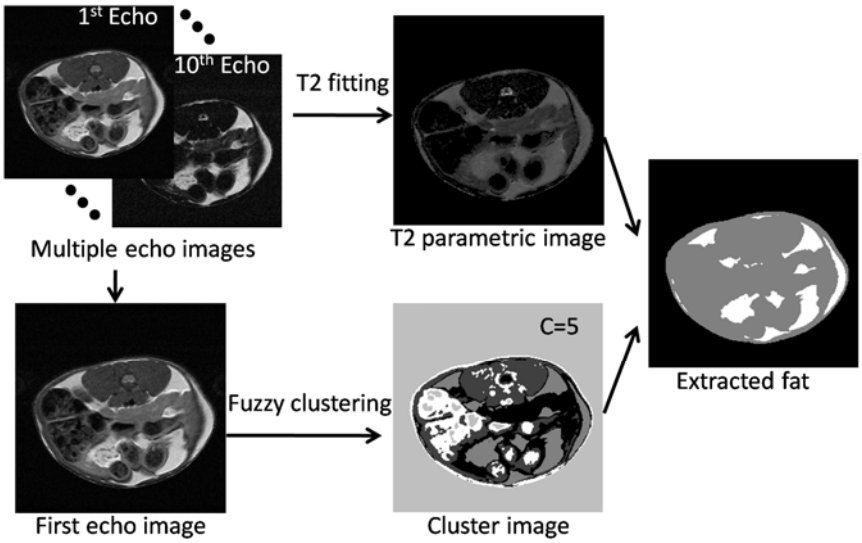

Fig. 3. The schematic representation of adipose measurement system using micro MRI.(Tang et al., 2011)

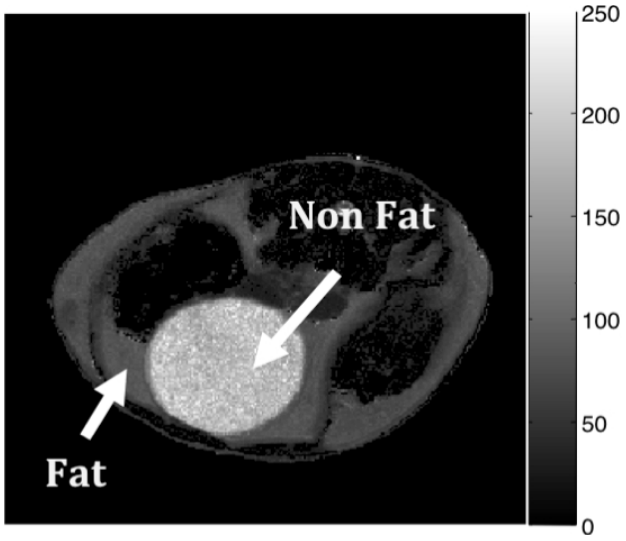

Fig. 4. The fat and non fat tissues in T2 parameter image.(Tang et al., 2011)

3.2 Image filter

The pre-processing step is necessary for reducing noise and thus enhance the image in specific ways. Filtering technique are often used for this purpose. Most image filters replaces the signal of a pixel according to the neighbouring pixels. Filtered image can be regarded as a convolution between original image and the kernel. The filter kernel, typically a matrix, represents the number of pixels nearby taken into account.

There are two typical filters including the linear and nonlinear filters used in image processing. The linear filter only takes into consideration the relative position in kernel, and remains constant throughout the whole image filtering. Nonlinear filters are relative to the target pixel and the coefficients are calculated as a function of local variations of the signal (Bonnya et al., 2003). For example, in the linear filter class, average and Gaussian filers are often used. Among the nonlinear filters, the median filter is popular. A selective blurring filter (Wang et al., 1981) is often used, which emphases the pixels with similar intensity to the target pixel. A bilateral filter (Tomasi&Manduchi, 1998) is an edge preserving technique proposed recently and has been widely used in image processing. In comparison to the selective blurring filter, not only the intensity similarity but also the spatial similarity is taken into account.

In this section, we try to give some examples of common filters for the adipose image and finally choose the bilateral filter for our system. Figure 5. shows the different results from both linear and nonlinear filters. For better insight, an amplified region of the whole image was displayed.

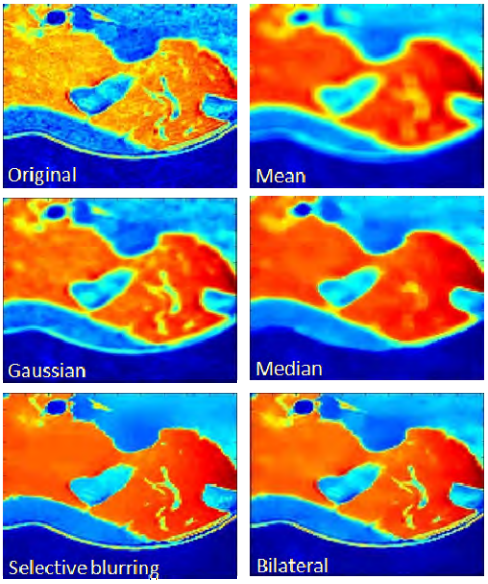

Fig. 5. The image of adipose tissue after the application of common image filters. (Tang et al., 2010)

3.3 Cluster image

Clustering is an important technique for image analysis, which can sort all the pixels in the image into different clusters according to their similarities. In our measurement system, the fuzzy c means (FCM) clustering approach (Dunn et al., 1973) was adopted to classify all pixels into groups and produce the cluster images. In this clustering, as shown in Figure 3 , the first echo image was chosen because of its relatively high SNR compared to later echo images.

In clustering, the cluster number is an important parameter. In the previous research (Positano et al., 2004; Positano et al., 2009; Ranefall et al., 2009), the cluster number was usually defined to be three, corresponding to background, fat and muscles. Nevertheless, in the real anatomy, more organs and tissues are included in the MR image. Three clusters do not well describe the discrepancies between different tissues. We found that increasing the cluster number was necessary to more accurately describe the full data. The fat tissue may display in multiple clusters and it becomes difficult to correctly select the appropriate cluster using intensity-only images. In our method, the clusters are recognized by their T2 values, which allowed us to increase the number of clusters.

3.4 T2 time

Transverse relaxation time (T2) is an important clue for adipose extraction in our system. To accurately measure the T2 time for each pixel of the parametric image, a curve is fitted to the decay of intensity with increasing TE (Vander et al., 2000). For the fitting of fat data, we used the weighted least square method with baseline subtraction and least point requirement. The fitting model and comparison of the fitting methods are described as follow.

3.4.1 Fitting model

The transverse relaxation time measurement of fat appears to satisfy a mono-exponential physical model known as: (Sijbers et al., 1998)

$$Si(S0,T2)=S0*\exp(-Tei/T2) \tag{1}$$

with Tei=i*te and S0 is the pseudo-proton density, which is relative to the true proton density, T1 value and receiver coil response.

3.4.2 Fitting methods

T2 value can be calculated by fitting the experimental data to above model in equation (1). To accomplish the fitting, a fitting method should be adopted. Here we have a comparison of the least square and weighted square method.

A least square method (LS) is the common way of fitting the curve, which consists in minimizing the quadratic distance between the fitted curve and the curve represented by the raw data.

$$\phi^2 = \sum_{i=1}^{N} [I_i - S_0 \exp(-Te_i / T_2)]^2 \tag{2}$$

Where I_i is the scanned intensity of intensity images in ith echo.

Weighted least square method (WLS) takes other factors into account using the weight with merit function:

$$\phi^2 = \sum_{i=1}^{N} w_i^2 [I_i - S_0 \exp(-Te_i / T_2)]^2 \tag{3}$$

Where w_i, the weight of ith point, should represent the confidence of the signal. As the low intensity signals are more likely to be noise and according have less certainty, here w_i was simply set as proportion to the intensity.

In figure 6, the calculated T2 and S0 in fitting model are compared using both least square and weighted least square methods. We can see that weighted least square method presents a more consist result compared to least square method. Therefore, we adopted the weighted least square method in our system.

3.5 Adipose separation

With T2 reference, the fat regions are extracted in the cluster image by comparing the clusters' similarities in T2 values. In order to take T2 into account, the average T2 values are calculated for each cluster. A similarity threshold Ts is defined:

$$Ts= | T2cluster-T2fat | / T2fat \tag{4}$$

Here the T2cluster is the average T2 value in each cluster from non-empty pixels and T2fat is the T2 value of fat.

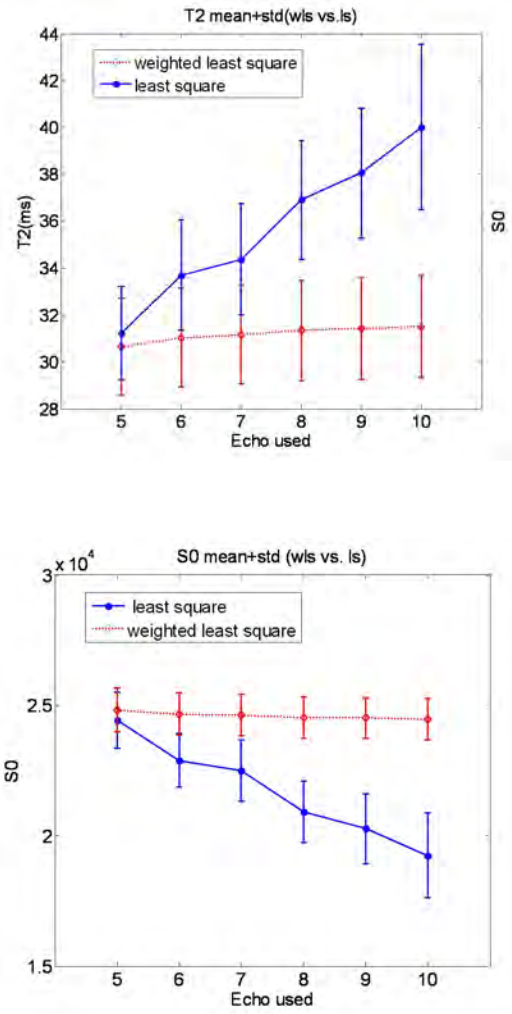

Fig. 6. Comparison of Methods for T2 fitting in the MR images(Tang et al., 2010)

Because the T2 value is related to the magnetic field strength, we suggest that the fat T2 could be defined by drawing a ROI in the known fat region or based on phantoms using the exact same imaging acquisition protocol and instrument.

The similarity threshold in Equation (4) defines a T2 range. The clusters with T2 value in the defined range are considered as fat tissues. Because the T2 values of fat and non-fat tissues are generally distinguishable, a reasonable threshold can be found for each specific application.

Instead of the threshold, a more complicate strategy can also be designed using a confidence image. More details can be found in our previous work (Tang et al., 2010).

4. Depot recognition

The definition of fat depots distribution and volume plays a great role in disease studies. In this study, we present a method to analysis the total adipose tissue (TAT), which employee a knowledge-based framework to separate the subcutaneous adipose tissue (SAT) from the visceral adipose tissue(VAT).

4.1 Principle

The basic procedures of depot separation are illustrated in Figure 7. Before the knowledge is applied, a morphological operation is performed to decompose the fat tissues. Then the unconnected parts are labelled and a knowledge-based method is adopted to recognize each object to be different depots.

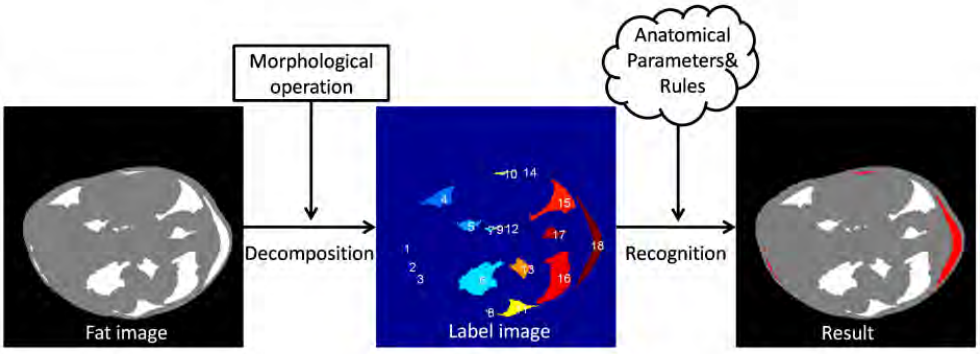

Fig. 7. The procedures of the depot recognition (Tang et al., 2011)

4.2 Decomposition

In the extracted fat image, the subcutaneous adipose tissues and visceral adipose tissues sometimes are accidently connected, which will complicate the depot recognition in further processing. Here a morphological opening operation (Gonzalez & Woods, 1992) is employed to decompose the adjoining parts. The morphological opening is composed by erosion and then dilation operations respectively. In our application, because some slim sections are erased by opening operation as well, the erased sections from pre- and post-morphological operation are saved for later placement into the mostly probable depot.

4.3 Knowledge based recognition

After decomposition, unconnected fat tissues are labelled as individual regions. To sort these individual regions into their likely respective fat depots, we employ a knowledge-based framework. Considering the variance of each feature, the descriptors are expressed by fuzzy logical (Zadeh, 1965). In the fuzzy set, each feature is assigned a grade of membership between 0 and 1. Using the fuzzy set to present the probability of belonging to different depots allows the anatomical variance to be contained in our system.

4.4 Parameters

Four parameters were adopted which contained the a priori knowledge of anatomical features. The parameters are described below and displayed in Figure. 8. (Tang et al., 2011)

4.4.1 Parameter 1: Orientation

Previous research indicates that the abdominal fat in mice tends to accumulate in a bilateral pattern (Calderan et al., 2006). Taking advantage of this a priori information, we implemented an orientation parameter dividing the body into bilateral regions and dorsal/ventral regions (Figure 9). The orientation parameter for each individual region in a polar system with its origin located at the geometrical centroid of the body area is as the mean of the maximum and minimum angles.

$$\text{Orientation}=(\text{maximum angle} + \text{minimum angle})/2$$

4.4.2 Parameter 2: Minimum distance

We define the feature of location, for each pixel inside the body area, which represents its distance to the nearest body contour. As Figure. 9 shows, a distance map is displayed for the inside the body area with the intensity corresponding to the distance. For example, the bright pixel near the centroid denotes a long distance to the body contour. The minimum distance parameter describes how close the outer edge of the fat region is to the body surface and is defined as the minimum value of the distance map in an individual region. This parameter is important for distinguishing the subcutaneous from visceral fat.

4.4.3 Parameter 3: Maximum distance

Similar to minimum distance, maximum distance is used to express the location feature that describes how far the fat tissues are away from the body surface. It is defined as the maximum value of the distance map in an individual region. Both minimum distance and maximum distance have three membership functions defining a confidence score for small, medium and large distance. Taking into consideration the observed regional variances (Calderan et al., 2006), different strategies are used in the bilateral and dorsal/ventral regions.

4.4.4 Parameter 4: Elongatedness

Elongatedness describes the shape of the object. Derived from empirical observations, in the band-like region near the body surface, the subcutaneous fat segments are usually slender along the surface; therefore a priori shape information is exploited in a location feature. An elongatedness parameter is defined to be the ratio of the length to thickness.

$$\text{Elongatedness}=\text{length}/\text{thickness}$$

Where (length=maximum angle-minimum angle) and (thickness=maximum distance-minimum distance).

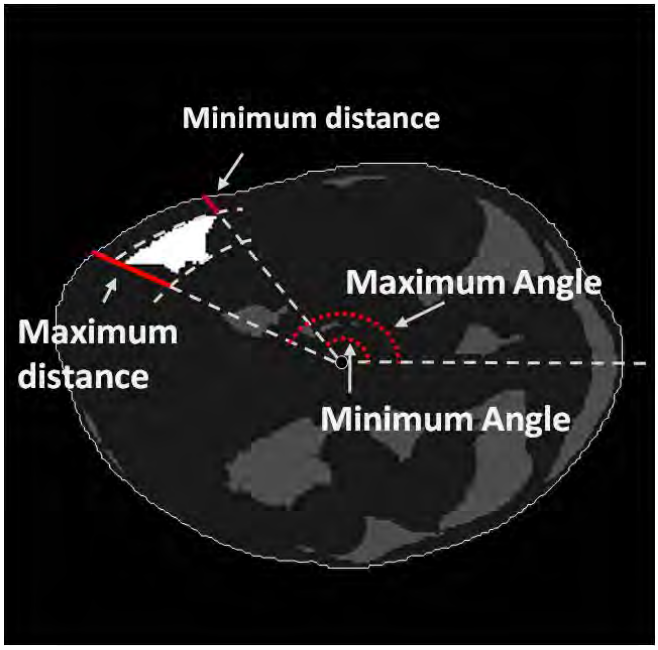

Fig. 8. The description of the parameters. (Tang et al., 2011)

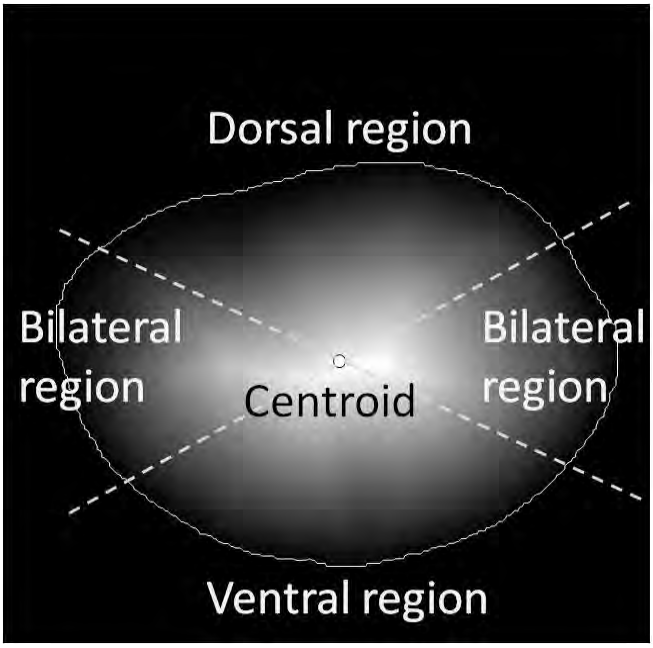

Fig. 9. The bilateral region and dorsal/ventral region. (Tang et al., 2011)

4.5 Inference rules

Utilizing the defined parameters, the depot can be recognized by classical If-Then rules and a min-max fuzzy inference scheme. Tissues are assigned to either the bilateral region or dorsal/ventral region (Fig.9) according to their orientations. Then three rules are employed to distinguish the depots:

Rule1: If maximum distance is small, then it is subcutaneous fat.
Rule2: If minimum distance OR maximum distance is large, then it is visceral fat.
Rule3: If minimum distance is small AND maximum distance is medium AND shape is elongated, then it is subcutaneous fat.

With defined rules, the min-max fuzzy inference scheme will automatically calculate the weights for each rule and assign the depot type in term of the weighted centroid (Zadeh, 1965).

5. Validation

To validate the measurement performed by the automatic process, we compared the automated results to the manual results from multiple observers.

5.1 Manual reference

In order to take inter-operator variations into account, two independent technicians performed the manual segmentations using a customized software tool developed in Matlab. In the software, two basic functions were provided including threshold and ROI analysis. The technicians first select the fat regions by adjusting a threshold. Then multiple manual ROI operations were performed to add or delete the fat regions based on the users experience. The total segmented fat is TAT. To segment the subcutaneous and visceral fat, operators carefully delineated a contour between these two depots. Finally, the fat inside the contour is considered as VAT and the rest of the fat is SAT.

5.2 Quantification results

The first comparison is for the segmented adipose size, which were performed in TAT, VAT and SAT respectively for all mice. A linear regression with 95% confidence ($P<0.001$) was calculated for each comparison. For the first manual result, the R2 for TAT is 0.953 with the regression function $y=1.088x+0.4407$; R2 for VAT is 0.9627 with the regression function $y=1.058x+1.769$; R2 for SAT is 0.8221 with the regression function $y=1.042x+0.8719$. For the second manual result, the R2 for TAT is 0.912 with the regression function $y=1.009x+6.583$; R2 for VAT is 0.9154 with the regression function $y=0.9889x+6.924$; R2 for SAT is 0.8986 with the regression function $y=1.037x+0.3821$. The agreement in the R2 value denotes the linear relationship between the automatic and manual results, and the concordance in the slope of the function provides confidence that the relationship will hold true in a variety of conditions. The agreement between the automatic results and manual results is comparable to the difference between correlation coefficients of the two manual results, which for TAT: R2=0.9514, VAT: R2=0.9195 and SAT: R2=0.8767.

A second comparison was performed to evaluate the voxel-by-voxel overlap of the segmented TAT, SAT and VAT respectively. To qualify these spatial similarities, we

adopted the dice coefficient, which is customarily used to compare the segmentation results in medical imaging.

As Equation 5 shows, the Dice Coefficient (DC) describes the average ratio of the intersection between the results (R1) and results (R2). For example, a complete overlap of the segment results will make the DC to be 1.

$$DC = \frac{2|R_1 \cap R_2|}{|R_1| + |R_2|} \tag{5}$$

We calculated the DC in the 26 mice for TAT, VAT and SAT respectively. The average value between automatic result and two manual results are for TAT: DC=0.8839, for VAT:DC= 0.8795 and for SAT:DC=0.873. The detailed statistic DC value (mean value ± standard deviation) for each result is displayed in Table 2. (Tang et al., 2011)

DC	TAT	VAT	SAT
A vs. M1	0.9087±0.0438	0.8999±0.0467	0.8783±0.0546
A vs. M2	0.8591±0.0558	0.840±0.0634	0.8677±0.0435
M1 Vs.M2	0.8846±0.052	0.8717±0.0598	0.8847±0.0491

Table 2. Dice Coefficient (DC) of automatic (A), first manual result (M1) and second manual result (M2). (Tang et al., 2011)

6. Conclusion

In this chapter, we introduce a adipose measurement system for small animal using micro MRI. We have presented the imaging protocol and technical detail of the post-processing methodology. The parameters are well defined yet adjustable and tuneable to new applications. By decreasing the amount of manual operation needed, we hope this technique can reduce the threshold for obesity researchers to use MRI in their research.

7. Acknowledgment

We would like to thank Richard Simerly for the experiments design and adipose research support. We thanks Susan Lee, Priyank Sharma and Marvin Nelson for input in the adipose measurement research. We also would like to thank Seda Mkhitaryan, Anahit Hovsepyan, Kevin Nelson, Harutyunyan Ira, Rozaliya Veytsman-Shpilberg, Vazgen Khankaldyyan and Karapetyan Gevorg for data acquisition/analysis and helpful discussions.

8. References

Bechah, Y.; Paddock,C.D.; Capo,C.; Mege,J.L.; Raoult, D.(2010). Adipose tissue serves as a reservoir for recrudescent Rickettsia prowazekii infection in a mouse model. *PLoS One* , 2010,vol.5,no.1,e.8547.

Bonnya, J.M.; Odile, B.T.; Michel, Z.; Jean-Pierre, R.(2003). Multi-exponential analysis of magnitude MR images using a quantitative multispectral edge preserving filter. *J. Magn. Reson*, 2003, Vol.161, pp.25-34.

Calderan,L.; Marzola, P.; Nicolato, E.; Fabene, P.F.; Milanese, C.; Bernardi, P.; Giordano, A.; Cinti, S.; Sbarbati, A. (2006). In vivo phenotyping of ob/ob mouse by magnetic resonance imaging and H-Magnetic resonance spectroscopy. *Obesity*,2006,Vol.14,pp.405–414.

Chae, Y., Jeong, M.G., Kim, D.(2007). Three dimensional volume measurement of mice abdominal fat in magnetic resonance images. e-Health Networking, *Application and Services*,2007,pp.252–255.

Church, C.; Lee, S.; Bagg, E.A.; McTaggart, J.S.; Deacon, R.; Gerken, T.; Lee, A.; Moir, L.; Mecinović, J.; Quwailid, M.M.; Schofield, C.J.; Ashcroft, F.M.; Cox, R.D.(2009). A mouse model for the metabolic effects of the human fat mass and obesity associated FTO gene. *PLoS Genet* ,2009,vol. 5, no.8, e.1000599.

Dixon, W.T. (1984). Simple proton spectroscopic imaging. *Radiology*,1984,Vol.153,pp.189-194.

Dunn J. C. (1973). A Fuzzy Relative of the ISODATA Process and Its Use in Detecting Compact Well-Separated Clusters, *Journal of Cybernetics*,1973, Vol.3, pp.32-57.

Gonzalez, R.C. & Woods, R.E. (1992). *Digital Image Processing*, 2nd edition, Addison-Wesley Longman Publishing, Boston,MA,1992.

Gray, D.S.; Fujioka, K.; Colletti, P.M.; et al.(1991). Magnetic resonance imaging used for determining fat distribution in obesity and diabetes. *Am J Clin Nutr* 1991, Vol.54, pp.623-627.

Gronemeyer, S.A.; Steen, R.G.; Kauffman, W.M.; Reddick, W.E.; Glass, J.O.(2000). Fast adipose tissue (FAT) assessment by MRI. *Magn Reson Imaging* 2000, Vol.18, pp.815-818.

Hou, Z.(2006). A review on mr image intensity inhomogeneity correction, *Int. J. Biomed. Imag*, 2006, pp.1-11.

Larsson, B.; Svärdsudd, K.; Welin, L.; Wilhelmsen, L.; Björntorp, P.; Tlibblin, G. (1984). Abdominal adipose tissue distribution, obesity and risk of cardiovascular disease and death: 13 y follow up of participants in the study of men born in 1913. *Br Med J Clin Res,* 1984, Vol 288,pp.1401-1404.

Lublinsky, S.; Luu, Y.K.; Rubin, C.T.; Judex, S.(2009). Automated separation of visceral and subcutaneous adiposity in in-vivo microcoputed tomographies of mice. *J Digit Imaging* 2009, Vol.22, pp.222-231.

Luu, YK; Lublinsky, S; Ozcivici E; et al.(2009). In vivo quantification of subcutaneous and visceral adiposity by micro-computed tomography in a small animal model. *Med Eng Phys* 2009, Vol.31, pp.34-41.

Mann, G.V. (1974). The Influence of Obesity in Health. *New England Journal of Medicine,* 1974, Vol. 291, pp.178–185.

Manson, J.E.; Colditz, G.A.; Stampfer, M.J.; et al.(1990). A Prospective Study of Obesity and Risk of Coronary Heart Disease in Women. *New England Journal of Medicine,* 1990, Vol.322, pp.882-889.

Ohshima, S.; Yamamoto, S.; Yamaji, T.; et al. (2008). Development of an Automated 3D Segmentation Program for Volume Quantification of Body Fat Distribution Using CT. *Nippon Hoshasen Gijutsu Gakkai Zasshi* 2008, Vol.64, pp.1177-1181.

Peng, Q.; McColl, R.W.; Wang, J.; Chia, J.M.; Weatherall, P.T.(2005). Water-saturated three-dimensional balanced steady-state free precession for fast abdominal fat quantification. *J Magn Reson Imaging*, 2005,Vol.21,pp. 263–271.

Positano, V.; Christiansen, T.; Santarelli, M.F.; Ringgaard, S.; Landini, L.; Gastaldelli, A. (2009). Accurate segmentation of subcutaneous and intermuscular adipose tissue from MR images of thigh. *J Magn Reson Imaging*,2009,Vol. 29, pp.677-684.

Positano, V.; Gastaldelli, A.; Sironi, A.M.; Santarelli, M.F.; Lombardi, M.; Landini, L.(2004). An accurate and robust method for unsupervised assessment of abdominal fat by MRI. *J Magn Reson Imaging*,2004,Vol. 20,No.4,pp. 684-689.

Ranefall, P.; Bidar, A.W.; Hockings, P.D.(2009) Automatric segmentation of intra-abdominal and subcutaneous adipose tissue in 3D whole Mouse MRI. J *Magn Reson Imaging*, 2009, Vol.30, No.3, pp.554-560.

Reeder,S.B.; Pineda, A. R.; Wen, Z.; Shimakawa, A.; Yu, H.; Brittain, J.H.; Gold, G.E.; Beaulieu, C.H.; Pelc, N.J.(2005). Iterative Decomposition of Water and Fat with Echo Asymmetry and Least-Squares Estimation (IDEAL): Application With Fast Spin-Echo Imaging. *Magnetic Resonance in Medicine*,2005,Vol. 54,pp.636–644.

Ross, R.; Aru, J.; Freeman, J.; Hudson, R.; Janssen, I.(2002). Abdominal adiposity and insulin resistance in obese men. *Am J Physiol Endocrinol Metab*, 2002, Vol.282, pp. 657-663.

Siegel, M.J.; Hildebolt, C.F.; Bae, K.T; et al.(2007). Total and Intra-abdominal Fat Distribution in Preadolescents and Adolescents: Measurement with MR Imaging. *Radiology,* 2007, Vol.242, No. 3, pp.846-856.

Sijbers, J.; Dden Dekker, A.J.; Verhoye, M.; Raman, E.; Van Dyck, D.(1998). Optimal estimation of T2 maps from magnitude MR images, *Proceedings of the SPIE Medical Imaging* 1998,Vol.3338, pp.384-390.

Snijder, M.B.; Van Dam, R.M.; Visser, M.; Seidell, J.C.(2006). What aspects of body fat are particularly hazardous and how do we measure them? *Int J Epidemiol* 2006, Vol. 35, pp.83-92.

Tang, Y.; Lee, S.; Nelson, M.D.; Simerly, R.; Moats,R.A.(2010). Adipose separation of small animal at 7T: a preliminary study. *BMC Genomics,* 2010, 11, S9.

Tang, Y.; Simerly, R.; Moats,R.A.(2011). An Automatic Technique for MRI Based Murine Abdominal Fat Measurement. *Radioengineering*., vol. 20, no. 4, p. 988-995.

Tomasi, C. & Manduchi, R.(1998). Bilateral Filtering for Gray and Color Images, *Proceedings of the IEEE International Conference on Computer Vision* 1998, pp.839-846.

Vovk, U.; Pernuŝ, F.; Likar, B.(2007). A review of methods for correction of intensity inhomogeneity in MRI. *IEEE Trans Med Imaging*. 2007,Vol.26,pp.405–21.

Wang, D. C.; Vagnucci, A. H.; Li, C.C.(1981). Gradient inverse weighted smoothing scheme and the evaluation of its performance. *Comput Graph Imaging Process,* 1981, Vol.15, pp.167–181.

Zadeh, L.A. (1965). Fuzzy sets. Inform Contr,1965,Vol. 8,pp.338-353.

Zhao, B.; Colville, J.; Kalaigian, J.; et al.(2006). Automated quantification of body fat distribution on volumetric computed tomography. *J Comput Assist Tomogr* 2006, vol.30, pp.777-783.